

## Discovery of Novel Allosteric Mitogen-Activated Protein Kinase Kinase (MEK) 1,2 Inhibitors Possessing Bidentate Ser212 Interactions

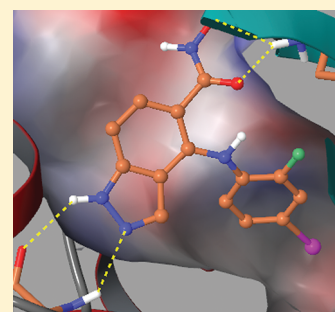
Robert A. Heald,<sup>\*,†</sup> Philip Jackson,<sup>†</sup> Pascal Savy,<sup>†</sup> Mark Jones,<sup>†</sup> Emanuela Gancia,<sup>†</sup> Brenda Burton,<sup>†</sup> Richard Newman,<sup>†</sup> Jason Boggs,<sup>‡</sup> Emily Chan,<sup>‡</sup> Jocelyn Chan,<sup>‡</sup> Edna Choo,<sup>‡</sup> Mark Merchant,<sup>‡</sup> Patrick Rudewicz,<sup>‡</sup> Mark Ultsch,<sup>‡</sup> Christian Wiesmann,<sup>‡</sup> Qin Yue,<sup>‡</sup> Marcia Belvin,<sup>‡</sup> and Steve Price<sup>†</sup>

<sup>†</sup>Argenta, 8/9 Spire Green Centre, Flex Meadow, Harlow, Essex CM19 5TR, U.K.

<sup>‡</sup>Genentech Inc., 1 DNA Way, South San Francisco, California 94080, United States

### S Supporting Information

**ABSTRACT:** Using structure-based design, two novel series of highly potent biaryl amine mitogen-activated protein kinase kinase (MEK) inhibitors have been discovered. These series contain an H-bond acceptor, in a shifted position compared with previously disclosed compounds, and an adjacent H-bond donor, resulting in a bidentate interaction with the Ser212 residue of MEK1. The most potent compound identified, **1** (G-894), is orally active in *in vivo* pharmacodynamic and tumor xenograft models.



### ■ INTRODUCTION

The Ras-Raf-MEK-ERK mitogen-activated protein kinase signaling pathway is one of the most promising targets for a new wave of molecularly targeted antitumor agents.<sup>1</sup> Constitutive activation of the extracellular regulated kinase (ERK) cascade, through oncogenic forms of Ras and mutations in B-Raf, has been observed in lung, colon, pancreas, kidney, and ovary primary human tumor samples.<sup>2</sup> Similarly, hyperactivity by upstream receptor tyrosine kinases such as human epidermal growth factor receptor 2 (HER2) leads to increased signaling through the ERK pathway.<sup>3</sup> Research efforts in recent years have uncovered a variety of inhibitors of Raf, MEK, and ERK kinases as potential antitumor agents.<sup>4</sup>

MEK is a crucial node in the ERK MAPK pathway: the only known downstream targets of MEK1/2 are ERK1/2. This has led to particularly intense efforts to discover inhibitors of this target, and there are now 13 MEK inhibitors at some stage of clinical evaluation for the treatment of cancer, with two others having been withdrawn.<sup>5,6</sup> The first MEK inhibitors to progress past phase I clinical trials were **2** (AZD6244/Selumetinib, Figure 1)<sup>7–9</sup> and PD325901,<sup>10</sup> both of which were progressed to phase II studies as single agents for the treatment of a variety of tumor types. Studies with **2** as a single agent and in combination with other antitumor agents are continuing.<sup>11</sup> The most advanced MEK inhibitor is GSK1120212,<sup>12</sup> which began a phase III trial in BRAF V600E positive melanoma patients in late 2010.

Although MEK inhibition alone is expected to provide significant therapeutic benefit, there is considerable evidence for synergistic combination with other targeted agents. For example, concerted MEK and PI3K inhibition provides

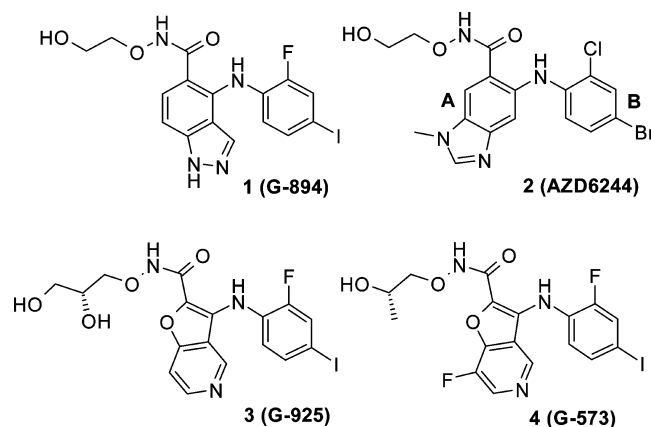


**Figure 1.** Structures of designed analogue **1** with **2**, **3**, and **4**. “A” and “B” rings of **2** are shown.

synergistic inhibition of tumor growth in basal-like breast cancer models.<sup>13</sup> Additionally, it has been demonstrated that in K-Ras mutant cell lines, Raf inhibition primes wild-type Raf to activate the Raf-MEK-ERK pathway, providing a clear rationale for combination therapy with MEK inhibitors.<sup>14</sup>

Allosteric MEK1/MEK2 inhibitors<sup>15</sup> are particularly discriminating kinase inhibitors. These compounds form a tertiary complex with the MEK enzyme and the ATP binding site and are thus uncompetitive.<sup>16,17</sup> The binding site for so-called type III kinase inhibitors is proximal to ATP and results in high

Received: December 20, 2011

Published: April 16, 2012

specificity for the target enzyme. It has been postulated that this allosteric “MEK pocket” may be present in other kinases.<sup>18</sup>

Examination of structural features of inhibitors disclosed in the patent literature reveals that the allosteric binding pocket of MEK1 is highly discriminating in its affinity for drug molecules, resulting in low structural diversity.<sup>15,19</sup> The structures of seven compounds that have entered the clinic have been disclosed: all are biaryl amines, by far the most common class of MEK inhibitor. The potency of these inhibitors is postulated to depend on three pharmacophoric elements (Figure 2).<sup>16</sup> The

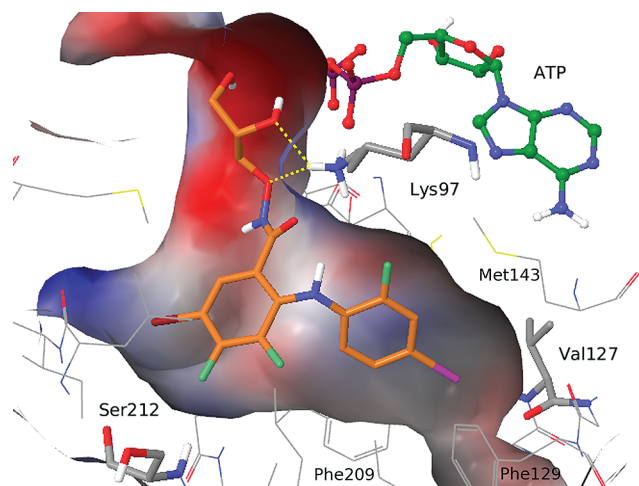


**Figure 2.** The key interactions of biarylaniline MEK inhibitors: crystal structure of MEK1 in complex with ATP (green) and PD318088 (orange) (PDB code 1S9J).

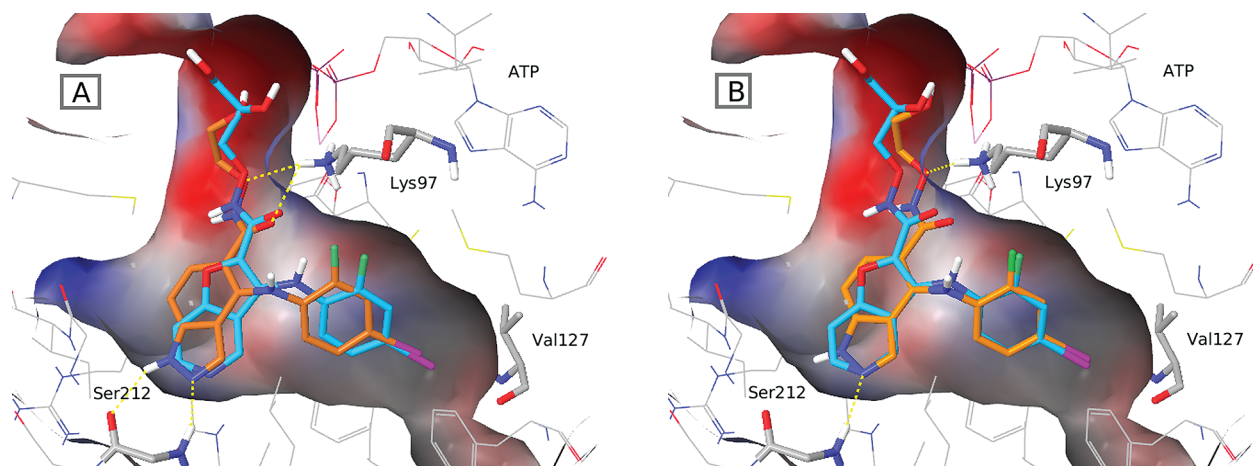
first of these is a “B-ring”, which occupies the lipophilic pocket formed by Leu118, Ile126, Val127, Ile141, Met143, Phe129, Phe209, and Val211, an important feature of which is para-substitution with a lipophilic polarizable atom or group capable of forming an interaction with the carbonyl of Val127. Where this atom is a halogen, the interaction is termed a halogen bond.<sup>20,21</sup> The second feature is a polar group which can interact with the terminal phosphate of ATP and Lys97, typically a hydroxamate, but sometimes an amide, reverse sulfonamide, or sulfonyl urea.<sup>22</sup> The third feature is an H-bond acceptor, which is suitably juxtaposed to Ser212. The strength

of this H-bond acceptor<sup>23</sup> and position relative to the aniline and hydroxamate are determined by the “A-ring” to which these moieties are attached. It has been proposed that increasing the strength of the Ser212/H-bond acceptor interaction results in greater tolerance in the other pharmacophoric elements.<sup>24</sup>

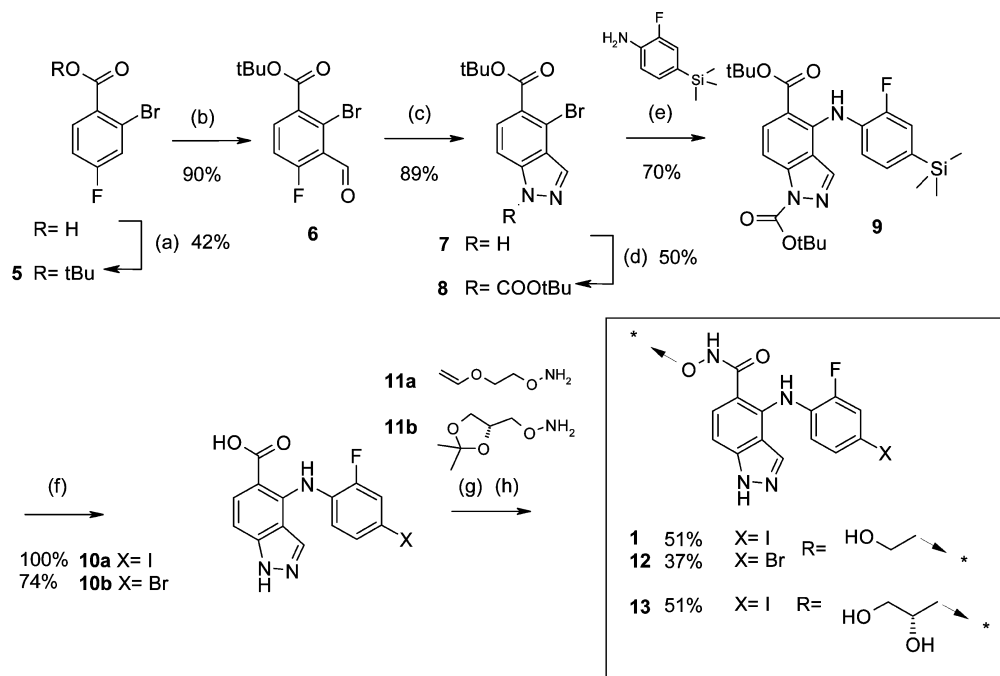
## RESULTS AND DISCUSSION

In our search for additional MEK inhibitors, we utilized a computer-aided drug design (CADD) driven approach leveraging key information from the X-ray crystal structure (2.7 Å resolution) of **3** (G-925, Figure 1), a compound from our first series of novel inhibitors<sup>25</sup> which was optimized to give the orally efficacious analogue **4** (G-573).<sup>26</sup> From 2-D overlay of **2** and **3**, it was noticed that the two A ring systems position the H-bond acceptor differently. Additionally, it was realized that for a 6,5-heterobicyclic system fusion of the five-membered ring toward the B-ring, in the opposite sense to **2**, together with movement of the acceptor round one position, placed the key pharmacophoric elements described above in remarkably similar position to **3**. An H-bond donor was added next to the acceptor, as it was postulated that this position would be proximal to the carbonyl of Ser212 resulting in the design of **1** (G-894, Figure 1). This designed compound is fundamentally different to all six-membered aryl and 6,5-fused biaryl amine MEK inhibitors disclosed in the literature in that the putative H-bond acceptor is not positioned on the six-membered ring meta to the aniline. Modeling of the indazole **1** in the **3**/MEK1 protein structure was performed using docking (Figure 3, A) and manual placement (Figure 3, B), as docking algorithms underestimate the iodine Val127 interaction. The docked pose shows bidentate Ser212 interaction, but the aniline ~1.3 Å out of the lipophilic pocket compared with **3**. In the manual overlay, the indazole acceptor was still appropriately positioned near Ser212, with the NH donor shifted slightly from the Ser212 carbonyl to a distance of 3.0 Å. Although neither pose of **1** was ideal, the protein movement required to enable all desired contacts is minimal.

It should be noted that it is not possible to achieve a formal bidentate Ser212 interaction using monoaryl or 6,5-fused biaryl MEK inhibitor scaffolds which have been previously disclosed. The possibility of identifying a MEK inhibitor making such a bidentate interaction with Ser212, which could lead to increased affinity, led us to target the synthesis of **1**.



**Figure 3.** (A) Overlay between the docked pose of **1** (orange) and the crystal structure of **3** (cyan, PDB code 3V01). (B) Overlay between **1** manually adjusted in the binding site (orange) and the crystal structure of **3** (cyan).

Scheme 1. Synthetic Route to Indazole Analogues 1 and 12<sup>a</sup>

<sup>a</sup>(a) (COCl)<sub>2</sub>, DMF, DCM, (ii) tBuOH, pyridine, DCM; (b) (i) LDA, THF, (ii) DMF; (c) N<sub>2</sub>H<sub>4</sub>·H<sub>2</sub>O DME, 90 °C; (d) Boc<sub>2</sub>O, Et<sub>3</sub>N, DCM; (e) Pd<sub>2</sub>dba<sub>3</sub>, xantphos, K<sub>3</sub>PO<sub>4</sub>, toluene, 90 °C; (f) (i) ICl, DCM or NBS, DCM, (ii) TFA, DCM; (g) EDCl, DIPEA, HOBt, DMF; (h) MeOH, HCl.

The desired 4-phenylamino-5-carboxylic acid core was synthesized following the route outlined in Scheme 1. Commercially available 2-bromo-4-fluorobenzoic acid was converted to the *tert*-butyl ester **5** under standard conditions. Regiospecific metalation with LDA followed by DMF quench gave aldehyde **6**. Cyclization of the *ortho*-fluoro aldehyde **6** to indazole **7** and subsequent reaction with boc-anhydride provided the appropriately substituted and protected indazole core **8**. Palladium-catalyzed amination with 2-fluoro-4-trimethylsilyl aniline using xantphos as the ligand<sup>25</sup> gave anilino ester **9**. Regiospecific iodination, directed by the trimethylsilyl group, followed by simultaneous boc-deprotection and ester hydrolysis, provided 4-(2-fluoro-4-iodo-phenylamino)-1*H*-indazole-5-carboxylic acid **10a**. Installation of the hydroxamate side-chain could then be achieved via a coupling reaction with vinyl hydroxylamine **11a** followed by acid-mediated deprotection. Bromo analogue **12** was prepared similarly from intermediate **9** using NBS rather than iodine monochloride for the halogenation step. Diol analogue **13** was also prepared from acid intermediate **10a**.

In a biochemical homogeneous time-resolved fluorescence (HTRF) assay, **1** was found to be ~2.5-fold more potent than **4** (Table 1), demonstrating that this designed analogue is a potent inhibitor of MEK. Potency was further assessed in HCT116 (K-Ras mutant human colorectal carcinoma cell line) and A375 (BRAF V600E mutant human melanoma cell line) cell lines, determining both the inhibition of ERK phosphorylation and cell proliferation. In these assays, **1** is consistently ~10-fold more potent than **4**. Bromo analogue **12** is less potent than **1**, as would be expected by reduction in strength of the Val127 halogen bond. However, **12** is equipotent with **4** in cellular assays, again demonstrating the excellent potency facilitated by the indazole scaffold. Results for **4** and **13** show a direct comparison between the azabenzofuran and indazole scaffolds. The indazole **13** is marginally more potent in the

**Table 1. Activity of Indazole Analogues 1, 12, and 13 Compared with Azabenzofurans 3 and 4**

compd	MEK HTRF IC <sub>50</sub> (nM)	P-ERK EC <sub>50</sub> (nM)		cell proliferation EC <sub>50</sub> (nM)	
		HCT116	A375	HCT116	A375
<b>1</b>	13	0.2	0.4	16	2
<b>3</b>	25	6.3	34.0	314	264
<b>4</b>	35	4.0	7.2	175	23
<b>12</b>	125	3.4	6.4	193	19
<b>13</b>	15	0.4	3.7	31	12

HTRF assay, equipotent in A375 cells, but much more potent in HCT116 cellular assays. The improved potency in cellular but not biochemical assays of the indazole compared with azabenzofurans is intriguing. As all of these compounds are uncompetitive with respect to ATP, it is understandable that cellular potency is greater than biochemical potency due to high intracellular concentrations of ATP. As the biochemical assay used a constitutively activated kinase construct, cellular data were taken to be more indicative of true potency. Differences in proliferation values between the two cell lines used are most likely due to differential sensitivity, as the shift between A375 and HCT116 cell lines is consistently 8–10-fold. **1** shows high specificity for MEK inhibition with <40% inhibition at 1 μM against a panel of 100 kinases (Invitrogen SelectScreen, see Supporting Information), indicating that inclusion of the indazole was not leading to promiscuous kinase hinge-binding.

An X-ray cocrystal structure (2.7 Å resolution) of **1** with MEK1 and ATP was obtained which confirmed the allosteric mode of binding and bidentate interaction with Ser212 (Figure 4, modeled hydrogen atoms shown for clarity) and a structure consistent with the manual overlay shown above (Figure 3, panel B). As expected, the iodo-aniline is positioned in the lipophilic pocket with the iodine atom ~3.3 Å from the

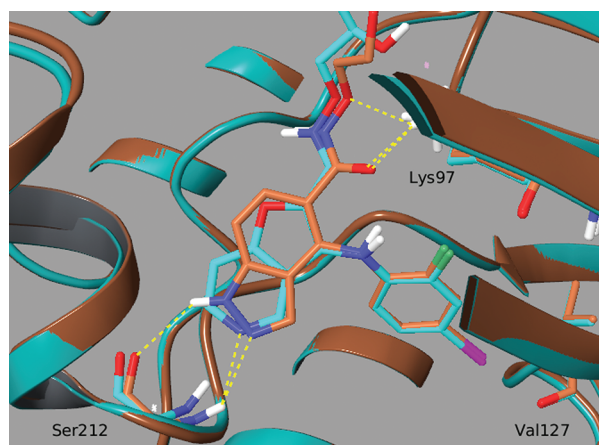


**Figure 4.** Crystal structure of **1** in complex with MEK1 (orange, PDB code 3V04); modeled hydrogens shown for clarity. For comparison, the crystal structure of MEK1 in complex with **3** is also shown (cyan).

carbonyl of Val127, an appropriate distance for formation of a halogen bond. With the aniline positioned ideally for lipophilic contacts and halogen bond, the indazole is able to make a donor–acceptor interaction with Ser212. The interatom distance for both the H-bonding atom pairs is 2.58 Å with angles of 134° and 142° for the indazole N Ser NH and indazole NH Ser CO interactions. Comparison with the crystal structure of **3** shows a small but significant induced-fit movement of Ser212 (when compared with the highly conserved positions of other residues in the pocket) which allows the three pharmacophoric elements to interact as desired: a shift of 0.48 Å is observed for the carbonyl oxygen. The shift in Ser212 to accommodate the donor–acceptor pair of **1** indicates that the postulated bidentate interaction exists and most adequately explains the potency of this compound.

When dosed in rats, the rate of clearance of **1** was found to be moderate ~2/3 liver blood flow (Table 2) and oral exposure and bioavailability were low. Similar results were found in mice where clearance was approximately equal to liver blood flow and oral exposure (AUC) was low. Low oral bioavailability in rat was attributed to high liver extraction ratio and poor solubility (solubility 0.08 mg/mL (pH 6.5), 0.18 mg/mL (FASSIF); measured MDCK permeability was moderate to high with low efflux (A:B 9.9 B:A  $13.8 \times 10^{-6}$  cm/s; ratio: 1.4). Analysis of plasma samples following oral dosing in rats showed that glucuronidation and cleavage of the hydroxamate to acid were the major routes of metabolism (see Supporting

Information). Bioavailability in mouse at 25 mg/kg was higher perhaps due to saturation of clearance mechanisms. The bromo analogue **12** was found to have higher clearance in rat than the iodo analogue despite lower lipophilicity, and bioavailability was found to be low. Diol hydroxamate **13** was not progressed into PK as it exhibited low MDCK cell permeability (A:B 2.0, B:A  $7.1 \times 10^{-6}$  cm/s efflux ratio 3.5). The azabenzofuran **4** has much lower clearance and higher oral exposure than **1** in mice.

Despite low oral exposure in rodents, the high potency of **1** in cellular assays warranted further investigation of this compound in an efficacy study. Gratifyingly, when dosed orally in nude HCT-116 tumor-bearing mice, **1** exhibited substantially greater efficacy at 5 mg/kg than **4** at the same dose (Figure 5),

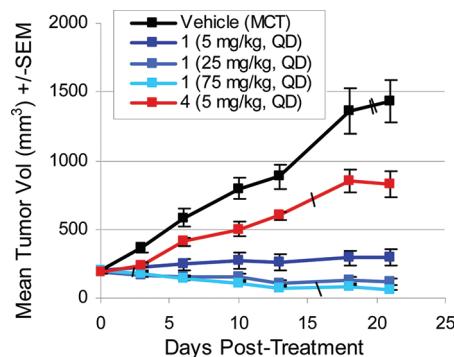


**Figure 5.** Efficacy in HCT116 colorectal xenograft model. Mice were randomized and treated with vehicle or **1** at 5, 25, and 75 mg/kg or **4** at 5 mg/kg, orally (PO) every day (QD) for 3 weeks. \ = death or euthanasia: 2 animals in the vehicle treated group had tumor volume >2000 mm<sup>3</sup>; animals euthanized in the compound treated groups had body weight loss >20%.

with tumor growth inhibition (TGI) approaching stasis (94%). The 5 mg/kg dose was well tolerated with no loss of body weight compared with vehicle (data not shown). At the 25 and 75 mg/kg doses, 5 and 10 out of 10 partial responses were observed but ~10% loss of body weight was noted at the higher dose. This improved efficacy compared with **4** can be largely attributed to increased potency. The free fraction for **1** in mice is ~2-fold higher than for **4**, which is perhaps within the error of the experiment, whereas the exposure of **1** is ~10-fold higher. Efficacy was found to correlate with inhibition of ERK phosphorylation in a separate pharmacodynamic experiment: a single dose of **1** at 25 mg/kg led to maximal inhibition of pERK

**Table 2. Rodent PK Data for 1, 4, and 12**

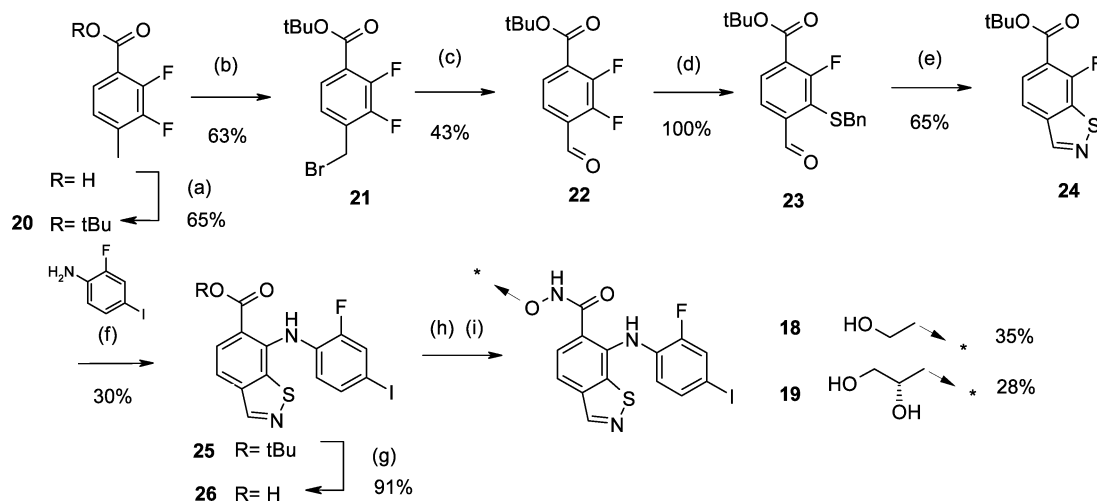
compound	species	PPB <sup>a</sup>	dose (mg/kg)/route	Cl <sup>b</sup> (mL/min/kg)	T <sub>1/2</sub> <sup>c</sup> (h)	Vd <sub>ss</sub> <sup>d</sup> (L/kg)	AUC <sup>e</sup> (μM·h)	F <sup>f</sup> (%)
<b>1</b>	rat	96.1	1/IV	36	1.4	2.4	1.01	
			5/PO <sub>(solution)</sub>				1.06	21
	mouse	97.0	1/IV	88	0.6	2.0	0.41	
			25/PO <sub>(suspension)</sub>		2.9		1.96	94
<b>4</b>	mouse	98.4	1/IV	7.7	2.3	0.71	4.42	
			25/PO <sub>(suspension)</sub>				192	173
<b>12</b>	rat	96.5	1/IV	54	0.36	1.5	0.75	
			5/PO <sub>(solution)</sub>				1.29	34

<sup>a</sup>Plasma protein binding. <sup>b</sup>Clearance. <sup>c</sup>Half-life. <sup>d</sup>Volume of distribution at steady state. <sup>e</sup>Area under the curve. <sup>f</sup>Bioavailability. For oral studies, MCT was used for suspension dosing and 60% PEG 400 for solution.

Table 3. Activity Data for Further Indazole Analogues

(i) RR'NH, EDCI, HOBT, DIPEA, THF, rt (ii) HCl, dioxan (**13** only)

Compound	MEK HTRF IC <sub>50</sub> (nM)	P-ERK EC <sub>50</sub> (nM)		Cell Proliferation EC <sub>50</sub> (nM)	
		HCT116	A375	HCT116	A375
<b>14</b>	79	1.5	1.5	127	9
<b>15</b>	93	1.3	2.4	132	4.9
<b>16</b>	>10,000	--	--	--	--
<b>17</b>	4546	--	--	--	--

Scheme 2. Synthetic Route to Benzoisothiazole Analogues<sup>a</sup>

<sup>a</sup>(a) Boc<sub>2</sub>O, DMAP, tBuOH, 45 °C; (b) NBS, AIBN, CCl<sub>4</sub>, reflux; (c) trimethylamine oxide, DCM, DMSO, rt; (d) BnSH, tBuOK, THF, -30 °C; (e) (i) SOCl<sub>2</sub>, DCM, rt, (ii) NH<sub>3</sub>, MeOH, THF, rt; (f) LHMDS, THF, -78 °C; (g) TFA, DCM, rt; (h) RONH<sub>2</sub>, EDCI, HOBT, DIPEA, THF, rt; (i) HCl, MeOH, rt.

(~70% of control values) through 8 h (see Supporting Information).

In an attempt to optimize the PK/potency balance, a number of analogues were prepared from acid intermediate **10a** that investigated variation of the hydroxamate group (Table 3). These analogues were assessed using in vitro or in vivo experiments as appropriate. Cyclopropylmethyl (**14**) and ethyl (**15**) hydroxamate analogues were found to be significantly less potent than **1**, and both showed no oral exposure when dosed at 5 mg/kg in rats (data not shown). Replacement of the hydroxamate with amides was not tolerated: **16** exhibited an IC<sub>50</sub> of >10 μM in the HTRF assay, and the azetidinol analogue **17** possessed very weak activity. In general, it appears that the indazole scaffold, despite enabling a bidentate donor–acceptor interaction with Ser212, is less tolerant of changes to the hydroxamate compared with previously disclosed pyridone monocyclic inhibitors.<sup>24</sup> This is perhaps due to less flexibility in positioning of the donor–acceptor element of the indazole compared with the monodentate pyridone.

Owing to the difficulty in balancing potency, metabolic stability, and oral bioavailability in the indazole series, our thoughts turned to other scaffolds that take advantage of our discovery of a bidentate Ser212 interaction and movement in the position of the H-bond acceptor. It has been postulated that the CH of some five-membered heterocycles can act as a weak H-bond donor.<sup>27,28</sup> Additionally, it is likely that our earlier azabenzofuran template is positioned appropriately to make a similar interaction. Replacing the fused pyrazole ring of **1** with an isothiazole would provide a system able to make a C–H···O donor–acceptor interaction with Ser212 with reduced polarity. It was considered that the lower energy of H-bond interaction may be compensated for by a reduced desolvation penalty compared with the indazole.

The synthesis of targeted analogues **18** and **19** (Scheme 2) depended on preparation of a benzoisothiazole with an unprecedented substitution pattern. The required intermediate, tetra-substituted derivative **22**, was prepared in two steps from ester **20** via radical bromination followed by oxidation with

trimethylamine oxide and DMSO. Regiospecific  $S_NAr$  displacement at the 3-position with phenylmethanethiol was achieved using potassium *tert*-butoxide at low temperature to furnish the desired compound **23**. The isothiazole ring was formed following a two-step procedure,<sup>29</sup> providing the 6,7-disubstituted benzisothiazole scaffold **24**. The 2-fluoro-4-iodoaniline was introduced through  $S_NAr$  displacement of the remaining fluorine atom using LHMDS at low temperature, giving the aniline ester **25**. Subsequent steps were carried out as for the indazole analogues.

Pleasingly, hydroxyethyl hydroxamate analogue **18** showed excellent potency in all assays and is only ~2–3-fold less potent than the direct indazole analogue **1** in P-ERK and cell proliferation assays (Table 4). These data prove that a formal

**Table 4. Activity Data for Benzisothiazole Analogues**

compd	MEK HTRF IC <sub>50</sub> (nM)	P-ERK EC <sub>50</sub> (nM)		cell proliferation EC <sub>50</sub> (nM)	
		HCT116	A375	HCT116	A375
<b>18</b>	15	0.6	0.9	44	7
<b>19</b>	20	0.9	1.1	62	10

H-bond donor on this novel 6,5-fused scaffold is not necessary for excellent potency. Diol analogue **19** is 2-fold less potent than indazole analogue **13** in the HTC116 cell proliferation assay and equipotent in A375 cells.

Calculated physicochemical properties for selected compounds with varying A-rings are shown in Table 5. These data show that cell shifts for both the benzisothiazole and indazole analogues are much reduced compared with azabenzofuran analogue **3**. Azabenzofuran analogue **4**, which has a less polar hydroxamate substituent and an A-ring substituted with fluorine, has more similar cell shifts to both benzisothiazoles and indazole **13**. High donor and acceptor count (>11) is the strongest correlate with increased cell shift; compare **1** and **13** and **3** and **4**, presumably due to reduced membrane permeability. This difference is more marked in A375 cells. From these data, it is apparent that the indazole and benzisothiazole scaffolds achieve increased cell potency by more optimal positioning of polar functionality.

When dosed in rats, compound **19** showed much reduced clearance and ~5-fold higher oral exposure compared with **1** (Table 6). However, as **19** is highly plasma protein bound, the unbound clearance is no better than for **1** (1875 cf. 923 mL/min/kg) and unbound oral AUC is very similar (0.046 cf. 0.040  $\mu$ M·h). As in the absence of active transport or restricted

permeability the unbound fraction of drugs drives efficacy, it was concluded that compound **19** does not improve on **1** and it was not tested further. Compound **18** was not progressed further, as it is a potent CYP2C9 and CYP2C19 inhibitor.

## CONCLUSION

In summary, using structure-based design leveraging key information from a previously disclosed azabenzofuran series, we have discovered novel allosteric MEK inhibitors which, partly through strengthened interaction with Ser212, display improved potency in cellular assays. The most potent compound discovered, indazole **1**, is efficacious at low doses in a human tumor xenograft model.

The relative contributions to potency of the C–H and N–H H-bond donors in the benzisothiazole and indazole scaffolds cannot be determined from comparison of the biochemical and cellular data presented here. However, it is clear that the H-bond acceptor of both these scaffolds is ideally positioned and facilitates excellent potency in either case. This result is at odds with previous evidence from the literature which suggests that the H-bond acceptor should be positioned next to the ring junction on 6,5-fused scaffolds, as in **2**. In this regard, the topology of MEK inhibitors such as **1** and **19** is unique. Additionally, taken together, the data on benzofuran, indazole, and benzisothiazole biaryl amine allosteric MEK inhibitors show that the design of the bicyclic A-ring is critical to achieving a balance of potency and desirable ADME properties. Further details of related compounds which build on these discoveries will be disclosed in due course.

## EXPERIMENTAL SECTION

**Chemistry. General Experimental Conditions.** All solvents and reagents were used as obtained. <sup>1</sup>H NMR spectra were recorded at ambient temperature using a Varian Unity Inova (400 MHz) spectrometer with a triple resonance 5 mm probe. Chemical shifts are expressed in ppm relative to tetramethylsilane.

LC-MS experiments to determine retention times ( $R_T$ ) and associated mass ions were performed using various methods which are fully described in the Supporting Information. Compounds **3** and **4** were prepared according to the patented procedures.<sup>25</sup> All final compounds were assessed for purity by LC-MS and found to be  $\geq$ 95% purity.

**2-Bromo-4-fluoro-benzoic Acid *tert*-Butyl Ester (**5**).** To a suspension of 2-bromo-4-fluoro-benzoic acid (28.5 g, 0.13 mol) in DCM (500 mL) at rt was added oxalyl chloride (11.35 mL, 0.26 mmol) followed by DMF (0.05 mL, catalytic, CARE vigorous gas evolution), and the reaction mixture stirred for 3 h. The reaction mixture was concentrated in vacuo and the residue dissolved in DCM (500 mL) before treatment with a solution of *tert*-butanol (28.5 g, 0.26

**Table 5. Physicochemical Properties for Selected Azabenzofuran, Indazole, And Benzisothiazole Analogues**

compd	scaffold	N <sub>Acc</sub> <sup>a</sup>	N <sub>Don</sub> <sup>b</sup>	TPSA <sup>c</sup>	ClogP <sup>d</sup>	HCT116 cell shift <sup>e</sup>	A375 cell shift <sup>f</sup>
<b>3</b>	azabenzofuran	8	4	117	2.11	13	11
<b>4</b>		7	3	97	3.42	5	0.65
<b>1</b>	indazole	7	4	99	3.32	1.2	0.15
<b>12</b>		7	4	99	3.06	1.5	0.15
<b>13</b>		8	5	120	2.49	2.0	0.8
<b>18</b>	benzisothiazole	6	3	84	3.67	3.1	0.50
<b>19</b>		7	4	104	2.84	2.9	0.47

<sup>a</sup>Number of hydrogen bond acceptors. <sup>b</sup>Number of hydrogen bond donors. <sup>c</sup>Topological polar surface area. <sup>d</sup>Calculated using Daylight v4.94. <sup>e</sup>(HCT cell proliferation EC<sub>50</sub>)/(MEK HTRF IC<sub>50</sub>). <sup>f</sup>(A375 cell proliferation EC<sub>50</sub>)/(MEK HTRF IC<sub>50</sub>).

Table 6. Rat PK Data for 19

compd	species	PPB <sup>a</sup>	dose (mg/kg)/route	Cl <sup>b</sup> (mL/min/kg)	T <sub>1/2</sub> <sup>c</sup> (h)	Vd <sub>ss</sub> <sup>d</sup> (L/kg)	AUC <sup>e</sup> (μM·h)	F <sup>f</sup> (%)
19	rat	99.2	1/IV	15	1.6	0.97	2.2	51
			5/PO <sub>(solution)</sub>				5.7	

<sup>a</sup>Plasma protein binding. <sup>b</sup>Clearance. <sup>c</sup>Half-life. <sup>d</sup>Volume of distribution at steady state. <sup>e</sup>Area under the curve. <sup>f</sup>Bioavailability. Vehicle for oral dosing: 60% PEG 400.

mol) and pyridine (20.5 g, 0.26 mol). The resultant mixture was stirred at rt for 3 days before it was diluted with DCM and washed (1 M aqueous sodium hydroxide, water, 0.1 M aqueous HCl, water), dried (Na<sub>2</sub>SO<sub>4</sub>), filtered, and concentrated in vacuo to give a yellow oil. The crude oil was subjected to flash chromatography (Si-PPC, gradient 0–20% ethyl acetate in cyclohexane) to give the title compound as a colorless oil (15.2 g, 42%). <sup>1</sup>H NMR (CDCl<sub>3</sub>, 400 MHz) δ ppm 7.76–7.73 (1H, m), 7.37 (1H, dd, *J* = 8.4, 2.5 Hz), 7.05 (1H, ddd, *J* = 8.7, 7.7, 2.5 Hz), 1.60 (9H, s).

**2-Bromo-4-fluoro-3-formyl-benzoic Acid *tert*-Butyl Ester (6).** To a cold (–78 °C) solution of diisopropylamine (11.3 mL, 80.3 mmol) in THF (200 mL) was added *n*-butyllithium (30 mL, 2.5 M in hexanes, 75 mmol), and the mixture stirred for 30 min. A solution of 2-bromo-4-fluoro-benzoic acid *tert*-butyl ester (20.0 g, 73 mmol) in THF (10 mL) was added dropwise, and the pale-orange solution stirred at –75 °C for 1.5 h. DMF (10.6 g, 146 mmol) was added, and the mixture stirred for a further 10 min before quenching with water. The products were partitioned between diethyl ether and water, and the organic layer was separated, washed with brine, dried (Na<sub>2</sub>SO<sub>4</sub>), filtered, and concentrated in vacuo to give the title compound as a yellow solid (20 g, 90%). <sup>1</sup>H NMR (CDCl<sub>3</sub>, 400 MHz) δ ppm 10.4 (1H, s), 7.80–7.73 (1H, m), 7.17 (1H, t, *J* = 9.1 Hz), 1.62 (9H, s).

**4-Bromo-1H-indazole-5-carboxylic Acid *tert*-Butyl Ester (7).** A biphasic solution of 2-bromo-4-fluoro-3-formyl-benzoic acid *tert*-butyl ester (19.5 g, 65 mmol), DME (80 mL), and hydrazine hydrate (30 mL) was heated at 90 °C for 1.5 h. After cooling, volatile solvent was removed in vacuo and the products were partitioned between ethyl acetate and saturated aqueous ammonium chloride. The organic extract was dried (Na<sub>2</sub>SO<sub>4</sub>), filtered, and concentrated in vacuo to give the title compound as a tan solid (17.2 g, 89%). LC-MS (method B): *R*<sub>T</sub> = 3.63 min, [M + CH<sub>3</sub>CN + H]<sup>+</sup> = 338/340, [M – H]<sup>–</sup> = 295/297. <sup>1</sup>H NMR (CDCl<sub>3</sub>) δ ppm 8.22 (1H, d, *J* = 1.0 Hz), 7.82 (1H, d, *J* = 8.7 Hz), 7.44 (1H, dd, *J* = 8.7, 1.0 Hz), 1.43 (9H, s).

**4-Bromo-indazole-1,5-dicarboxylic Acid di-*tert*-Butyl Ester (8).** To a solution of 4-bromo-1H-indazole-5-carboxylic acid *tert*-butyl ester (12.0 g, 40 mmol) and triethylamine (6.1 mL, 44 mmol) in DCM (200 mL) was added di-*tert*-butyl-dicarbonate (9.6 g, 44 mmol), and the reaction mixture stirred at rt for 18 h. The reaction mixture was diluted with DCM, washed (saturated aqueous NaHCO<sub>3</sub>, water), dried (Na<sub>2</sub>SO<sub>4</sub>), filtered, and concentrated in vacuo in the presence of diatomaceous earth. The crude product was subjected to flash chromatography (Si-PPC, gradient 0–10% ethyl acetate in cyclohexane) to give the title compound as an off-white solid (8.5 g, 50%). <sup>1</sup>H NMR (CDCl<sub>3</sub>) δ ppm 8.29 (1H, s), 8.18–8.10 (1H, m), 7.92 (1H, d, *J* = 8.7 Hz), 1.70 (9H, s), 1.63 (9H, s).

**4-(2-Fluoro-4-trimethylsilylphenylamino)indazole 1,5-Dicarboxylic Acid di-*tert*-Butyl Ester (9).** A solution of 2-fluoro-4-trimethylsilylphenylamine (4.4 g, 24 mmol) in toluene (80 mL) was added to a mixture of 4-bromo-indazole-1,5-dicarboxylic acid di-*tert*-butyl ester (8.0 g, 20 mmol), Pd<sub>2</sub>dba<sub>3</sub> (456 mg, 2.5 mol %), xantphos (576 mg, 5 mol %), and potassium phosphate tribasic (5.96 g, 28 mmol) under nitrogen. The atmosphere was evacuated and backfilled with nitrogen, and then the reaction mixture heated at 100 °C for 4 h. The cooled reaction mixture was diluted with ethyl acetate, filtered through Celite, and the filtrate concentrated in vacuo. The resultant residue was subjected to flash chromatography (Si-PPC, dry loading on diatomaceous earth, gradient 0–10% ethyl acetate in cyclohexane) to give a solid which was triturated in methanol to give the title compound as a white solid (7.02 g, 70%). <sup>1</sup>H NMR (CDCl<sub>3</sub>) δ ppm 10.03 (1H, s), 8.05 (1H, d, *J* = 9.0 Hz), 7.57 (1H, dd, *J* = 9.0, 0.8 Hz), 7.28–7.18 (4H, m), 1.68 (9H, s), 1.63 (9H, s), 0.28 (9H, s).

**4-(2-Fluoro-4-iodophenylamino)-1H-indazole-5-carboxylic Acid (10a).** To a solution of 4-(2-fluoro-4-trimethylsilylphenylamino)-indazole-1,5-dicarboxylic acid di-*tert*-butyl ester (5.0 g, 10 mmol) in DCM (20 mL) at 0 °C was added iodine monochloride as a solution in DCM (20 mL, 1N, 20 mmol). The reaction mixture was stirred at 0 °C for 15 min and then diluted with saturated aqueous sodium thiosulfate solution (10 mL) and extracted with DCM. The combined organic extracts were washed with water, dried (Na<sub>2</sub>SO<sub>4</sub>), and concentrated in vacuo to yield the title compound as a tan foam. The foam was dissolved in DCM (25 mL) and TFA (15 mL) added. The reaction mixture was stirred at rt for 2 h before being concentrated in vacuo. The resultant residue was triturated in cyclohexane to give the title compound as a gray–pink solid (4.1 g, quantitative). LC-MS (method B): *R*<sub>T</sub> = 3.23 min, [M + H]<sup>+</sup> = 398. <sup>1</sup>H NMR (DMSO-*d*<sub>6</sub>) δ ppm 10.2 (1H, s), 7.84 (1H, d, *J* = 8.9 Hz), 7.78 (1H, d, *J* = 9.9 Hz), 7.58 (1H, d, *J* = 8.3 Hz), 7.16 (1H, t, *J* = 8.5 Hz), 7.02 (1H, s), 6.96 (1H, d, *J* = 8.9 Hz).

**4-(2-Fluoro-4-iodophenylamino)-1H-indazole-5-carboxylic Acid (2-vinyloxyethoxy)-amide.** To a solution of 4-(2-fluoro-4-iodophenylamino)-1H-indazole-5-carboxylic acid (2.14 g, 5.39 mmol) and *O*-(2-vinyloxy-ethyl)-hydroxylamine (668 mg, 6.50 mmol) in DMF (50 mL) was added EDCI hydrochloride (1.14 g, 5.93 mmol), HOBt (0.80 g, 5.93 mmol), and DIPEA (1 mL, 5.93 mmol). The reaction mixture was stirred at rt for 2 h before being concentrated in vacuo. The resultant residue was dissolved in ethyl acetate (30 mL), washed with aqueous saturated sodium bicarbonate solution (300 mL), and the aqueous phase extracted with ethyl acetate (2 × 20 mL). The combined organic extracts were washed with brine (30 mL), dried (MgSO<sub>4</sub>), filtered, and concentrated in vacuo. The resultant residue was subjected to flash chromatography (SiO<sub>2</sub>, gradient 0–100% ethylacetate in cyclohexane) to give the title compound as a pale-yellow solid (1.85 g, 71%). LC-MS (method B): *R*<sub>T</sub> = 3.52 min, [M – H]<sup>+</sup> = 481. <sup>1</sup>H NMR (CD<sub>3</sub>OD) δ ppm 7.57 (1H, dd, *J* = 10.2, 1.9 Hz), 7.53 (1H, d, *J* = 8.7 Hz), 7.45 (1H, ddd, *J* = 8.4, 1.9, 1.1 Hz), 7.37 (1H, s), 7.07 (1H, d, *J* = 8.8 Hz), 6.96 (1H, t, *J* = 8.6 Hz), 6.50 (1H, dd, *J* = 14.3, 6.8 Hz), 4.23 (1H, dd, *J* = 14.4, 2.05 Hz), 4.16–4.15 (2H, m), 3.99–3.99 (3H, m).

**4-(2-Fluoro-4-iodophenylamino)-1H-indazole-5-carboxylic Acid (2-Hydroxyethoxy)-amide (1).** To a solution of 4-(2-fluoro-4-iodophenylamino)-1H-indazole-5-carboxylic acid (2-vinyloxyethoxy)-amide (1.85 g, 3.84 mmol) in methanol (40 mL) was added hydrochloric acid (3 mL, 1N, 3 mmol). The reaction mixture was stirred at rt for 1 h, during which an off-white solid precipitated. The reaction mixture was concentrated in vacuo and the residue triturated with hot methanol/water (10 mL, 1:1). The product was collected by filtration and dried in vacuo to yield the title compound as an off white solid (1.26 g, 72%). LC-MS (method A): *R*<sub>T</sub> = 8.28 min, [M + H]<sup>+</sup> = 457. <sup>1</sup>H NMR (DMSO-*d*<sub>6</sub>) δ ppm 13.20 (1H, s), 11.61 (1H, s), 9.93 (1H, s), 7.66 (1H, dd, *J* = 10.3, 1.9 Hz), 7.46 (1H, d, *J* = 8.8 Hz), 7.42 (1H, dd, *J* = 8.5, 1.8 Hz), 7.24 (1H, s), 7.01 (1H, d, *J* = 8.8 Hz), 6.91 (1H, t, *J* = 8.6 Hz), 4.68 (1H, s), 3.85 (2H, dd, *J* = 5.4, 4.5 Hz), 3.56 (2H, t, *J* = 4.8 Hz). HRMS: calculated isotopic *M*<sub>w</sub> (M + Na), 478.9992; observed isotopic *M*<sub>w</sub> (M + Na), 479.0080; confirmed formula, C<sub>16</sub>H<sub>14</sub>FIN<sub>4</sub>O<sub>3</sub>; high resolution error, 18.4 ppm.

**2,3-Difluoro-4-methyl-benzoic Acid *tert*-Butyl Ester (20).** A mixture of 2,3-difluoro-4-methyl-benzoic acid (20.0 g, 116 mmol), di-*tert*-butyl dicarbonate (25.0 g, 116 mmol), and DMAP (2.0 g, 16.4 mmol) in *tert*-butanol (500 mL) was stirred at 45 °C for 5 h before being concentrated in vacuo. The resultant residue was triturated in diethyl ether and filtered. The filtrate was concentrated in vacuo to give a residue which was partitioned between ethyl acetate and a 1 M

aqueous solution of hydrochloric acid. The organic layer was separated and washed with a saturated aqueous solution of sodium hydrogen carbonate followed by brine, dried ( $\text{Na}_2\text{SO}_4$ ), filtered, and concentrated in vacuo to give the title compound as a colorless oil (17.3 g, 65%).  $^1\text{H NMR}$  ( $\text{CDCl}_3$ )  $\delta$  ppm 7.51 (1 H, ddd,  $J = 8.3, 6.6, 1.9$  Hz), 6.95 (1 H, m), 2.33 (3 H, d,  $J = 2.3$  Hz), 1.59 (9 H, s).

**4-Bromomethyl-2,3-difluoro-benzoic Acid *tert*-Butyl Ester (21).** A solution of 2,3-difluoro-4-methyl-benzoic acid *tert*-butyl ester (17.3 g, 75.9 mmol) and *N*-bromosuccinimide (13.5 g, 75.9 mmol) in carbon tetrachloride (250 mL) was degassed for 10 min. AIBN (1.2 g, 7.32 mmol) was added, and the reaction mixture was stirred at reflux for 18 h before being cooled to rt and filtered. The filtrate was concentrated in vacuo to give a residue which was subjected to flash chromatography (Si-PPC, gradient 0–10% TBME in cyclohexane) to afford the title compound as a colorless oil (16.7 g, contaminated by 25% of starting material).  $^1\text{H NMR}$  ( $\text{CDCl}_3$ )  $\delta$  ppm 7.61 (1 H, ddd,  $J = 8.3, 6.4, 2.1$  Hz), 7.18 (1 H, ddd,  $J = 8.1, 6.4, 1.8$  Hz), 4.49 (2 H, d,  $J = 1.3$  Hz), 1.59 (9 H, s).

**2,3-Difluoro-4-formyl-benzoic Acid *tert*-Butyl Ester (22).** To a solution of 4-bromomethyl-2,3-difluoro-benzoic acid *tert*-butyl ester (12.9 g, 42.1 mmol) in DMSO (80 mL) and DCM (40 mL) at 0 °C was added trimethylamine *N*-oxide (3.4 g, 45.3 mmol). The reaction mixture was stirred at rt for 18 h before being concentrated in vacuo. The resultant residue was partitioned between iced water and ethyl acetate. The organic layer was separated and washed with brine twice, dried ( $\text{Na}_2\text{SO}_4$ ), filtered, and evaporated in vacuo. The resultant residue was subjected to flash chromatography (Si-PPC, gradient 0–10% TBME in cyclohexane) to afford the title compound as a white solid (4.34 g, 43%).  $^1\text{H NMR}$  ( $\text{CDCl}_3$ )  $\delta$  ppm 10.38 (1 H, d,  $J = 0.8$  Hz), 7.71 (1 H, dddd,  $J = 7.4, 5.6, 1.7, 0.8$  Hz), 7.63 (1 H, ddd,  $J = 7.4, 5.6, 1.5$  Hz), 1.61 (9 H, s).

**3-Benzylsulfanyl-2-fluoro-4-formyl-benzoic Acid *tert*-Butyl Ester (23).** To a solution of potassium *tert*-butoxide (2.0 g, 17.9 mmol) in anhydrous THF (80 mL) was added benzyl mercaptan (2.1 mL, 17.9 mmol). The reaction mixture was stirred at rt for 5 min before being cooled to –30 °C. A solution of 2,3-difluoro-4-formyl-benzoic acid *tert*-butyl ester (4.34 g, 17.9 mmol) in anhydrous THF (20 mL) was added dropwise over 15 min, and the resultant mixture was stirred at –30 °C for 30 min before being quenched by addition of water and extracted with ethyl acetate. The organic layer was separated, washed with water followed by brine, dried ( $\text{Na}_2\text{SO}_4$ ), filtered, and concentrated in vacuo to give the title compound as a yellow oil (6.2 g, 100%).  $^1\text{H NMR}$  ( $\text{CDCl}_3$ )  $\delta$  ppm 10.20 (1 H, d,  $J = 0.6$  Hz), 7.84 (1 H, ddd,  $J = 8.0, 6.8, 0.7$  Hz), 7.59 (1 H, dd,  $J = 8.0, 0.9$  Hz), 7.19 (3 H, m), 7.05 (2 H, m), 4.07 (2 H, s), 1.63 (9 H, s).

**7-Fluoro-benzo[d]isothiazole-6-carboxylic Acid *tert*-Butyl Ester (24).** To a solution of 3-benzylsulfanyl-2-fluoro-4-formyl-benzoic acid *tert*-butyl ester (6.20 g, 17.9 mmol) in DCM (100 mL) was added sulfur chloride (2.9 mL, 35.8 mmol). The reaction mixture was stirred at rt for 1 h before being concentrated in vacuo. The resultant residue was azeotroped with toluene twice and then taken up in THF (50 mL). The resultant solution was cooled to 0 °C, and a 2 M solution of ammonia in methanol (100 mL) was added. The reaction mixture was stirred at rt for 1 h and then concentrated in vacuo. The resultant residue was partitioned between ethyl acetate and a saturated aqueous solution of sodium hydrogen carbonate. The organic layer was separated and washed with water followed by brine, dried ( $\text{Na}_2\text{SO}_4$ ), filtered, and evaporated in vacuo. The residue was subjected to flash chromatography (Si-PPC, gradient 0–10% diethyl ether in pentane) to give the title compound as a yellow solid (2.96 g, 65%).  $^1\text{H NMR}$  ( $\text{CDCl}_3$ )  $\delta$  ppm 8.93 (1 H, dd,  $J = 4.1, 0.5$  Hz), 7.91 (1 H, ddd,  $J = 8.3, 5.8, 0.5$  Hz), 7.84 (1 H, d,  $J = 8.3$  Hz), 1.64 (9 H, s).

**7-(2-Fluoro-4-iodo-phenylamino)-benzo[d]isothiazole-6-carboxylic Acid *tert*-Butyl Ester (25).** To a solution of 7-fluoro-benzo[d]isothiazole-6-carboxylic acid *tert*-butyl ester (1.26 g, 5.0 mmol) and 2-fluoro-4-iodo-phenylamine (1.18 g, 5.0 mmol) in anhydrous THF (25 mL) at –78 °C was added a 1.0 M solution of LHMDS in hexanes (10.0 mL, 10.0 mmol) under a nitrogen atmosphere. The reaction mixture was allowed to warm to rt and then stirred for 30 min before being quenched by the addition of a

saturated aqueous solution of ammonium chloride and extracted with ethyl acetate. The organic layer was separated and washed with water followed by brine, dried ( $\text{Na}_2\text{SO}_4$ ), filtered, and evaporated in vacuo. The residue was subjected to flash chromatography (Si-PPC, gradient 0–10% TBME in cyclohexane) to give the title compound as a yellow solid (717 mg, 30%). LC-MS (method B):  $R_T = 5.14$  min,  $[\text{M} + \text{H}]^+ = 471$ .  $^1\text{H NMR}$  ( $\text{CDCl}_3$ )  $\delta$  ppm 9.85 (1 H, s), 8.77 (1 H, s), 7.99 (1 H, dd,  $J = 8.6, 0.5$  Hz), 7.49–7.48 (3 H, m), 6.90 (1 H, t,  $J = 8.3$  Hz), 1.65 (9 H, s).

**7-(2-Fluoro-4-iodo-phenylamino)-benzo[d]isothiazole-6-carboxylic Acid (26).** To a solution of 7-(2-fluoro-4-iodo-phenylamino)-benzo[d]isothiazole-6-carboxylic acid *tert*-butyl ester (710 mg, 1.51 mmol) in DCM (5 mL) were added water (0.15 mL) and TFA (5 mL). The reaction mixture was stirred at rt for 1 h before being concentrated in vacuo. The resultant residue was azeotroped with toluene to give the title compound as a yellow solid (571 mg, 91%). LC-MS (method B):  $R_T = 3.95$  min,  $[\text{M} + \text{H}]^+ = 415$ .  $^1\text{H NMR}$  ( $\text{CDCl}_3$ )  $\delta$  ppm 9.69 (1 H, s), 8.79 (1 H, s), 8.08 (1 H, d,  $J = 8.6$  Hz), 7.55–7.54 (2 H, m), 7.49 (1 H, d,  $J = 8.6$  Hz), 7.01 (1 H, t,  $J = 8.3$  Hz).

**7-(2-Fluoro-4-iodo-phenylamino)-benzo[d]isothiazole-6-carboxylic Acid (2-Vinyloxy-ethoxy)-amide.** To a solution of 7-(2-fluoro-4-iodo-phenylamino)-benzo[d]isothiazole-6-carboxylic acid (328 mg, 0.79 mmol) and DIPEA (0.41 mL, 2.37 mmol) in DMF (2 mL) were added *O*-(2-vinyloxy-ethyl)-hydroxylamine (163 mg, 1.58 mmol), EDCI (303 mg, 1.58 mmol), and HOBt (213 mg, 1.58 mmol). The reaction mixture was stirred for 18 h at rt and then diluted with ethyl acetate and washed with water, then a saturated aqueous solution of sodium bicarbonate, and then brine before being dried ( $\text{Na}_2\text{SO}_4$ ), filtered, and concentrated in vacuo. The resultant residue was subjected to flash chromatography (Si-PPC, gradient 0–100% TBME in cyclohexane) to afford the title compound as a yellow foam (194 mg, 49%). LC-MS (method B):  $R_T = 3.99$  min,  $[\text{M} + \text{H}]^+ = 500$ .  $^1\text{H NMR}$  ( $\text{CDCl}_3$ )  $\delta$  ppm 9.38 (1 H, s), 8.99 (1 H, s), 8.81 (1 H, s), 8.29–6.73 (2 H, m), 6.82 (1 H, t,  $J = 8.8$  Hz), 6.53 (1 H, dd,  $J = 14.4, 6.8$  Hz), 4.33 (2 H, m), 4.24 (1 H, m), 4.11 (1 H, m), 4.03 (2 H, m).

**7-(2-Fluoro-4-iodo-phenylamino)-benzo[d]isothiazole-6-carboxylic Acid (2-Hydroxy-ethoxy)-amide (18).** To a solution of 7-(2-fluoro-4-iodo-phenylamino)-benzo[d]isothiazole-6-carboxylic acid (2-vinyloxy-ethoxy)-amide (187 mg, 0.37 mmol) in methanol (4 mL) was added a 1.0 M aqueous solution of hydrochloric acid (0.75 mL, 0.75 mmol). The reaction mixture was stirred at rt for 1 h before being concentrated under reduced pressure. The residue was taken up in ethyl acetate and washed with a saturated aqueous solution of sodium bicarbonate and brine, dried ( $\text{Na}_2\text{SO}_4$ ), filtered, and concentrated in vacuo. The residue was subjected to flash chromatography (Si-PPC, gradient 0–100%, ethyl acetate in DCM) to give the title compound as a yellow solid (128 mg, 72%). LC-MS (method A):  $R_T = 9.81$  min,  $[\text{M} + \text{H}]^+ = 474$ .  $^1\text{H NMR}$  ( $\text{CDCl}_3$ )  $\delta$  ppm 9.33 (1 H, s), 8.86 (1 H, s), 8.77 (1 H, s), 7.55–7.40 (4 H, m), 6.84 (1 H, t,  $J = 8.3$  Hz), 4.10 (2 H, t,  $J = 4.2$  Hz), 3.91 (1 H, t,  $J = 6.4$  Hz), 3.80 (2 H, t,  $J = 4.5$  Hz).

**7-(2-Fluoro-4-iodo-phenylamino)-benzo[d]isothiazole-6-carboxylic Acid ((*R*)-2,2-Dimethyl-[1,3]dioxolan-4-ylmethoxy)-amide.** To a solution of 7-(2-fluoro-4-iodo-phenylamino)-benzo[d]isothiazole-6-carboxylic acid (377 mg, 0.91 mmol) and DIPEA (0.47 mL, 2.73 mmol) in DMF (4 mL) were added *O*-((*R*)-2,2-dimethyl-[1,3]dioxolan-4-ylmethyl)-hydroxylamine (268 mg, 1.82 mmol), EDCI (349 mg, 1.82 mmol), and HOBt (246 mg, 1.82 mmol). The reaction mixture was stirred for 18 h at rt before being diluted with ethyl acetate. The resultant solution was washed with water followed by a saturated aqueous solution of sodium hydrogen carbonate and then brine before being dried ( $\text{Na}_2\text{SO}_4$ ), filtered, and concentrated in vacuo. The resultant residue was subjected to flash chromatography (Si-PPC, gradient 0–100% TBME in cyclohexane) to give the title compound as a yellow solid (266 mg, 54%). LC-MS (method B):  $R_T = 4.04$  min,  $[\text{M} + \text{H}]^+ = 544$ .  $^1\text{H NMR}$  ( $\text{CDCl}_3$ )  $\delta$  ppm 8.88 (1 H, s), 8.63 (1 H, s), 8.28 (1 H, s), 7.04 (1 H, d,  $J = 8.3$  Hz), 6.98 (1 H, dd,  $J = 9.5, 1.9$

Hz), 6.94 (2 H, m), 6.30 (1 H, t,  $J = 8.3$  Hz), 3.96 (1 H, m), 3.62–3.60 (3 H, m), 3.35 (1 H, m), 0.95 (3 H, s), 0.88 (3 H, s).

**7-(2-Fluoro-4-iodo-phenylamino)-benzo[d]isothiazole-6-carboxylic Acid ((R)-2,3-Dihydroxy-propoxy)amide (19).** To a solution of 7-(2-fluoro-4-iodo-phenylamino)-benzo[d]isothiazole-6-carboxylic acid ((R)-2,2-dimethyl-[1,3]dioxolan-4-ylmethoxy)-amide (263 mg, 0.48 mmol) in methanol (10 mL) was added a 1.0 M aqueous solution of hydrochloric acid (0.97 mL). The reaction mixture was stirred at rt for 18 h before being concentrated in vacuo. The resultant residue was taken up in ethyl acetate, washed with a saturated aqueous solution of sodium hydrogen carbonate and then brine, dried ( $\text{Na}_2\text{SO}_4$ ), filtered, and concentrated in vacuo. The resultant residue was subjected to flash chromatography (Si-PPC, gradient 0–100% ethyl acetate in DCM) to give the title compound as a yellow solid (127 mg, 53%). LC-MS (method A):  $R_T = 9.05$  min,  $[\text{M} + \text{H}]^+ = 504$ .  $^1\text{H}$  NMR ( $\text{CD}_3\text{OD}$ )  $\delta$  ppm 8.88 (1 H, s), 7.74 (1 H, d,  $J = 8.4$  Hz), 7.61 (1 H, d,  $J = 8.3$  Hz), 7.53 (1 H, dd,  $J = 10.0, 1.9$  Hz), 7.44 (1 H, ddd,  $J = 8.4, 1.9, 1.1$  Hz), 6.76 (1 H, t,  $J = 8.5$  Hz), 4.05 (1 H, dd,  $J = 10.0, 3.5$  Hz), 3.96–3.83 (2 H, m), 3.63–3.52 (2 H, m). HRMS: calculated isotopic  $M_w$  ( $\text{M} + \text{Na}$ ), 525.9710; observed isotopic  $M_w$  ( $\text{M} + \text{Na}$ ), 525.9601; confirmed formula,  $\text{C}_{17}\text{H}_{15}\text{FIN}_3\text{O}_4\text{S}$ ; high resolution error,  $-20.07$  ppm.

**In Vitro Methods for the Determination of MEK Inhibition, Cellular Levels of Phospho-ERK, and Cell Proliferation.** *MEK1 Inhibition Assay.* A homogeneous time-resolved fluorescence assay (HTRF) was used to test for inhibition of kinase activity. A constitutively active MEK1 was obtained from Invitrogen and was tested at a concentration of 15 nM with 50  $\mu\text{M}$  ATP, 50 nM inactive ERK1, and the test compound in a 25 mM HEPES buffer, pH 7.5, containing 10 mM  $\text{MgCl}_2$ , 5 mM  $\beta$ -glycerophosphate, 0.1 mM sodium orthovanadate, and 0.1 mg/mL Triton X 100. The kinase assay was carried out for 30 min at 25 °C and was terminated by the addition of EDTA. HTRF reagents (CisBio) were added and time-resolved fluorescence was read using a Wallac Victor V (Perkin-Elmer).  $\text{IC}_{50}$  values quoted are the result of at least two separate determinations where the results were within 2-fold of each other and were calculated using the KLfit software package (version 2.0.5).

*Assay for Cellular Levels of Phospho-ERK.* Cells (HCT116 or A375) were seeded at 26700/well into collagen-coated 96-well plates and were incubated overnight under normal tissue culture conditions. The following day, the cells were exposed to MEK inhibitors for 2 h. At the end of this time, the cells were fixed and permeabilized by incubation in 2% formaldehyde for 45 min followed by 100% ice-cold methanol for 10 min. The fixed and permeabilized cells were washed with PBS and blocked with 3% BSA in Tris buffered saline plus Tween 20 (TBST) for 1 h at 37 °C. At the end of this time, the blocking solution was replaced with an antiphospho-ERK antibody raised in rabbit (New England Biolabs) at a dilution of 1:1000 made in blocking solution and the cells were incubated overnight at 4 °C, followed by washing and incubation with anti-rabbit-Ig- Alexa Flour 488 (Invitrogen) at a dilution of 1:1000 in blocking solution for 2 h at rt. Following washing, the cells were incubated with 1.5  $\mu\text{M}$  propidium iodide for 2 h in the dark and read on a high content imager (Acumen, TTP LabTech) in the red and green channels to measure P-ERK content and cell number.  $\text{EC}_{50}$  values quoted are the result of at least two separate determinations, where the results were within 2-fold of each other and were calculated using the KLfit software package (version 2.0.5).

*Cell Proliferation Assay.* Cells (HCT116 or A375) were seeded at 26700/well into collagen-coated 96-well plates and were incubated overnight under normal tissue culture conditions. The following day, the cells were exposed to MEK inhibitors for 72 h under normal tissue culture conditions. At the end of this time, the cells were equilibrated to rt and mixed 1:1 with Cell Titer Glo reagent prepared as indicated by the supplier (Promega), followed by a 10 min incubation. Luminescence was read using a TopCount (Perkin-Elmer).  $\text{EC}_{50}$  values quoted are the result of at least two separate determinations, where the results were within 2-fold of each other and were calculated using the KLfit software package (version 2.0.5).

**Molecular Modeling Methods.** All molecular modeling experiments were carried out using software from Schrödinger Inc. The crystal structure of MEK1 (extracted from the cocrystal with **3**, PDB reference 3V01) was prepared using the Protein Preparation Wizard in Maestro (Protein Preparation Wizard, Schrödinger, LLC, New York, NY), which assigns bond orders, adds hydrogen atoms, deletes water molecules, and generates appropriate protonation states. The prepared protein structure was then minimized using OPLS2001 (until the rmsd reached 0.3 Å) and used to generate the receptor grids for docking. The binding site was defined using the native ligand and selecting the option “docking ligands similar in size”. The ligand structures were built in Maestro and prepared for docking using LigPrep 2.0 (LigPrep, Schrödinger, LLC, New York, NY). The docking experiments were carried out with Glide 4.0<sup>30</sup> in Extra Precision mode, using the default parameters setting. The top five docking poses for each ligand were selected and visually inspected.

**X-Ray Crystal Structure Determination Method.** *Cloning and Expression.* The truncated (residues 63–393)MEK1 was cloned from a wt MEK1 full length construct via PCR and subcloned into pET24b (Novagen) as previously described.<sup>16</sup> The recombinant MEK1 was expressed in *Escherichia coli* (Rosetta 2 pLys S) and grown in Ultra Yield Flasks (Thomson Instrument Company) TB media/MOPS/glycerol at 37 °C to an O.D. of 1 (600 nm). The cells were then placed at 16 °C and induced after 30 min with 0.5 mM IPTG and allowed to grow an additional 18 h.

*Protein Purification and Crystallization.* MEK1 was purified using Cobalt immobilized metal affinity resin (TALON), ion exchange, and size exclusion chromatography. The protein was concentrated to 15 mg/mL and incubated with 10-fold molar excess inhibitor plus 1 mM MgAMP-PNP before crystallization. MEK1 crystals grew from hanging drop vapor diffusion using 12% w/v PEG 8000, 0.4 M  $\text{NH}_4\text{H}_2\text{PO}_4$ , and 0.1 M HEPES pH 6.9 at 18 °C. MEK1 crystals belonging to the space group P62 and unit cell  $a = 81$  Å and  $c = 129$  Å were previously described.<sup>16</sup>

*Structure Determination and Refinement.* Synchrotron data was collected at the Advanced Light Source (ALS) beamline 5.0.2. Diffraction data to 2.7 Å at 100 K was processed using HKL2000<sup>31</sup> suite of programs. Molecular replacement was performed using MOLREP in CCP4<sup>32</sup> suite with PDB accession code 1S9J as the starting model. Refinement was conducted using REFMAC5.2. The refinement statistics are summarized in the Supporting Information.

## ■ ASSOCIATED CONTENT

### § Supporting Information

Methods and further results for the in vivo pharmacodynamic and efficacy studies involving **1**; experimental procedures for the preparation of compounds **12–17**; NMR spectra for **1** and **19**; data collection and refinement statistics for complexes of **3** and **1** with MEK1; kinase panel data for **1**; rat in vivo metabolite identification for **1**. This material is available free of charge via the Internet at <http://pubs.acs.org>.

### Accession Codes

The coordinates for the crystal structures of **1** and **3** with MEK1 have been deposited with the RCSB Protein Data Bank under the accession codes 3V04 and 3V01, respectively.

## ■ AUTHOR INFORMATION

### Corresponding Author

\*Phone: +44 (0) 1279 645623. Fax: +44 (0) 1279 645646. E-mail: [robert.heald@glpg.com](mailto:robert.heald@glpg.com).

### Notes

The authors declare no competing financial interest.

## ■ ACKNOWLEDGMENTS

We thank Kirk Robarge, Mark Zak, and Paul Gibbons for helpful discussions and collection of experimental data.

## ■ ABBREVIATIONS USED

AMP-PNP, adenylyl-imidodiphosphate; DIPEA, diisopropylethylamine; EDCI, 1-ethyl-3-(3'-dimethylaminopropyl)-carbodiimide hydrochloride; HEPES, 4-(2-hydroxyethyl)-1-piperazineethanesulfonic acid; HOBt, 1-hydroxybenzotriazole; IPTG, isopropyl- $\beta$ -D-thiogalactopyranoside; MDCK, Madin-Darby canine kidney cells; MOPS, 3-(N-morpholino)propanesulfonic acid; Pd<sub>2</sub>dba<sub>3</sub>, tris-(dibenzylideneacetone)-dipalladium(0); SEM, standard error of the mean; Si-PPC, prepacked silica flash chromatography cartridge (Isolute SPE, Biotage SNAP or ISCO Rediseq); TBME, *tert*-butyl methyl ether; xantphos, 4,5-bis(diphenylphosphino)-9,9-dimethylxanthene

## ■ REFERENCES

- Roberts, P. J.; Der, C. J. Targeting the Raf-MEK-ERK mitogen-activated protein kinase cascade for the treatment of cancer. *Oncogene* **2007**, *26*, 3291–3310.
- Hoshino, R.; Chantani, Y.; Yamori, T.; Tsuruo, T.; Oka, H.; Yoshida, O.; Shimada, Y.; Ari-I, S.; Wada, H.; Fujimoto, J.; Kohno, M. Constitutive activation of the 41-/43-kDa mitogen-activated protein kinase signaling pathway in human tumors. *Oncogene* **1999**, *18*, 813–822.
- Olayioye, M. A.; Neve, R. M.; Lane, H. A.; Hynes, N. E. The ErbB signaling network: receptor heterodimerization in development and cancer. *EMBO J.* **2000**, *19*, 3159–3167.
- Sebolt-Leopold, J. S. Advances in the development of cancer therapeutics directed against the RAS-mitogen-activated protein kinase pathway. *Clin. Cancer Res.* **2008**, *14*, 3651–3656.
- Thomson Reuters Integrity; Thomson Reuters: East Haven, CT; <http://integrity.prouds.com/> (Accessed December 10, 2011).
- Frémin, C.; Meloche, S. From basic research to clinical development of MEK1/2 inhibitors for cancer therapy. *J. Hematol. Oncol.* **2010**, *3*, 8.
- Yeh, T. C.; Marsh, V.; Bernat, B. A.; Ballard, J.; Colwell, H.; Evans, R. J.; Parry, J.; Smith, D.; Brandhuber, B. J.; Gross, S.; Marlow, A.; Hurley, B.; Lyssikatos, J.; Lee, P. A.; Winkler, J. D.; Koch, K.; Wallace, E. Biological characterization of ARRY-142886 (AZD6244), a potent, highly selective mitogen-activated protein kinase kinase 1/2 inhibitor. *Clin. Cancer Res.* **2007**, *13*, 1576–1583.
- Davies, B. R.; Logie, A.; McKay, J. S.; Martin, P.; Steele, S.; Jenkins, R.; Cockerill, M.; Cartledge, S.; Smith, P. D. AZD6244 (ARRY-142886), a potent inhibitor of mitogen-activated protein kinase/extracellular signal-regulated kinase 1/2 kinases: mechanism of action in vivo, pharmacokinetic/pharmacodynamic relationship, and potential for combination in preclinical models. *Mol. Cancer Ther.* **2007**, *6*, 2209–2219.
- Adjei, A. A.; Cohen, R. B.; Franklin, W.; Morris, C.; Wilson, D.; Molina, J. R.; Hanson, L. J.; Gore, L.; Chow, L.; Leong, S.; Maloney, L.; Gordon, G.; Simmons, H.; Marlow, A.; Litwiler, K.; Brown, S.; Poch, G.; Kane, K.; Haney, J.; Eckhardt, S. G. Phase I pharmacokinetic and pharmacodynamic study of the oral, small-molecule mitogen-activated protein kinase kinase 1/2 inhibitor AZD6244 (ARRY-142886) in patients with advanced cancers. *J. Clin. Oncol.* **2008**, *26*, 2139–2146.
- Barrett, S. D.; Bridges, A. J.; Dudley, D. T.; Saltiel, A. R.; Fergus, J. H.; Flamme, C. M.; Delaney, A. M.; Kaufman, M.; LePage, S.; Leopold, W. R.; Przybranowski, S. A.; Sebolt-Leopold, J.; Van Becelaere, K.; Doherty, A. M.; Kennedy, R. M.; Marston, D.; Howard, W. A., Jr.; Smith, Y.; Warmus, J. S.; Tecle, H. The discovery of the benzhydroxamate MEK inhibitors CI-1040 and PD0325901. *Bioorg. Med. Chem.* **2008**, *18*, 6501–6504.
- ClinicalTrials.gov; National Institutes of Health: Bethesda, MD; <http://www.clinicaltrials.gov/ct2/results?term=AZD6244> (Accessed December 10, 2011).
- Abe, H.; Kikuchi, S.; Hayakawa, K.; Iida, T.; Nagahashi, N.; Maeda, K.; Sakamoto, J.; Matsumoto, N.; Miura, T.; Matsumura, K.; Seki, N.; Inaba, T.; Kawasaki, H.; Yamaguchi, T.; Kakefuda, R.; Nanayama, T.; Kurachi, H.; Hori, Y.; Yoshida, T.; Kakegawa, J.; Watanabe, Y.; Gilmartin, A. G.; Richter, M. C.; Moss, K. G.; Laquerre, S. G. Discovery of a Highly Potent and Selective MEK Inhibitor: GSK1120212 (JTP-74057 DMSO Solvate). *ACS Med. Chem. Lett.* **2011**, *2* (4), 320–324.
- Hoeflich, K. P.; O'Brien, C.; Boyd, Z.; Cavet, G.; Guerrero, S.; Jung, K.; Januario, T.; Savage, H.; Punnoose, E.; Truong, T.; Zhou, W.; Berry, L.; Murray, L.; Amler, L.; Belvin, M.; Friedman, L. S.; Lackner, M. R. In Vivo Antitumor Activity of MEK and Phosphatidylinositol 3-Kinase Inhibitors in Basal-Like Breast Cancer Models. *Clin. Cancer Res.* **2009**, *14*, 4649–4664.
- Hatzivassiliou, G.; Song, K.; Yen, I.; Brandhuber, B. J.; Anderson, D. J.; Alvarado, R.; Ludlam, M. J. C.; Stokoe, D.; Gloor, S. L.; Vigers, G.; Morales, T.; Aliagas, I.; Liu, B.; Sideris, S.; Hoeflich, K. P.; Jaiswal, B. J.; Seshagiri, S.; Koeppen, H.; Belvin, M.; Friedman, L. S.; Malek, S. RAF inhibitors prime wild-type RAF to activate the MAPK pathway and enhance growth. *Nature* **2010**, *464*, 431–435.
- Price, S. Putative allosteric MEK1 and MEK2 inhibitors. *Expert Opin. Ther. Pat.* **2008**, *18*, 603–627.
- Ohren, J. F.; Chen, H.; Pavlovsky, A.; Whitehead, C.; Zhang, E.; Kuffa, P.; Yan, C.; McConnell, P.; Spessard, C.; Banotai, C.; Mueller, W. T.; Delaney, A.; Omer, C.; Sebolt-Leopold, J. S.; Dudley, D. T.; Leung, I. K.; Flamme, C.; Warmus, J.; Kaufman, M.; Barrett, S.; Tecle, H.; Hasemann, C. A. Structures of human MAP kinase kinase 1 (MEK1) and MEK2 describe novel noncompetitive kinase inhibition. *Nature Struct. Mol. Biol.* **2004**, *11*, 1192–1197.
- Fischmann, T. O.; Smith, C. K.; Mayhood, T. W.; Myers, J. E., Jr.; Reichert, P.; Mannarino, A.; Carr, D.; Zhu, H.; Wong, J.; Yang, R.; Le, H. V.; Madison, V. S. Crystal structures of MEK1 binary and ternary complexes with nucleotides and inhibitors. *Biochemistry* **2009**, *48*, 2661–2674.
- Tecle, H.; Shao, J.; Li, Y.; Kothe, M.; Kazmirski, S.; Penzotti, J.; Ding, Y.-H.; Ohren, J.; Moshinsky, D.; Coli, R.; Jhavar, N.; Bora, E.; Jacques-O'Hagan, S.; Wu, J. Beyond the MEK-pocket: Can current MEK kinase inhibitors be utilized to synthesize novel type III NCKIs? Does the MEK-pocket exist in kinases other than MEK? *Bioorg. Med. Chem. Lett.* **2009**, *19*, 226–229.
- Trujillo, J. I. MEK Inhibitors: a patent review. *Expert Opin. Ther. Pat.* **2011**, *21* (7), 1045–1069.
- Politzer, P.; Lane, P.; Concha, M. C.; Ma, Y.; Murray, J. S. An overview of halogen bonding. *J. Mol. Model.* **2007**, *13*, 305–311.
- Voth, A. R.; Ho, P. S. The role of halogen bonding in inhibitor recognition and binding by protein kinases. *Curr. Top. Med. Chem.* **2007**, *7*, 1336–1348.
- Iverson, C.; Larson, G.; Lai, C.; Yeh, L.-T.; Dadson, C.; Weingarten, P.; Appleby, T.; Vo, T.; Maderna, A.; Vernier, J. M.; Hamatake, R.; Miner, J. N.; Quart, B. RDEA119/BAY 869766: A potent, selective, allosteric inhibitor of MEK1/2 for the treatment of cancer. *Cancer Res.* **2009**, *69*, 6839–6847.
- Laurence, C.; Brameld, K. A.; Graton, J.; Le Questel, J. Y.; Renault, E. The pK<sub>BHX</sub> database: toward a better understanding of hydrogen-bond basicity for medicinal chemists. *J. Med. Chem.* **2009**, *52*, 4073–4086.
- Wallace, E. M.; Lyssikatos, J.; Blake, J. F.; Seo, J.; Yang, H. W.; Yeh, T. C.; Perrier, M.; Jarski, H.; Marsh, V.; Poch, G.; Livingston, M. G.; Otten, J.; Hingorani, G.; Woessner, R.; Lee, P.; Winkler, J.; Koch, K. Potent and selective mitogen-activated protein kinase kinase (MEK) 1,2 inhibitors. 1. 4-(4-Bromo-2-fluorophenylamino)-1-methylpyridin-2(1H)-ones. *J. Med. Chem.* **2006**, *49*, 441–444.
- Price, S.; Williams, K.; Savy, P. P.; Dyke, H. J.; Montana, J. G.; Stanley, M. S.; Bao, L. Aza-benzofuran compounds and methods of use. Patent WO2008024725, 2008.
- Choo, E. F.; Belvin, M.; Chan, J.; Hoeflich, K.; Orr, C.; Robarge, K.; Yang, X.; Zak, M.; Boggs, J. Preclinical disposition and pharmacokinetics—pharmacodynamic modeling of biomarker response and tumour growth inhibition in xenograft mouse models of G-573, a MEK inhibitor. *Xenobiotica* **2010**, *11*, 751–762.

(27) Pierce, A. C.; Sandretto, K. L.; Bemis, G. W. Kinase inhibitors and the case for CH...O hydrogen bonds in protein–ligand binding. *Proteins* **2002**, *49*, 567–576.

(28) Toth, G.; Bowers, S. G.; Truong, A. P.; Probst, G. The role and significance of unconventional hydrogen bonds in small molecule recognition by biological receptors of pharmaceutical relevance. *Curr. Pharm. Des.* **2007**, *13*, 3476–3493.

(29) Fink, D. M.; Strupczewski, J. T. Process and intermediates for the preparation of 6-fluorobenzoisothiazoles. *Can. Pat. Appl. CA 2076556*, 1993.

(30) Friesner, R. A.; Banks, J. L.; Murphy, R. B.; Halgren, T. A.; Klicic, J. J.; Mainz, D. T.; Repasky, M. P.; Knoll, E. H.; Shelley, M.; Perry, J. K.; Shaw, D. E.; Francis, P.; Shenkin, P. S. Glide: A new approach for rapid, accurate docking and scoring. 1. Method and assessment of docking accuracy. *J. Med. Chem.* **2004**, *47*, 1739–1749.

(31) Otwinowski, Z.; Minor, W. Processing of X-ray Diffraction Data Collected in Oscillation Mode. *Methods Enzymol.* **1997**, *276*, 307–326.

(32) The CCP4 suite: programs for protein crystallography Collaborative Computational Project, Number 4. *Acta Crystallogr., Sect. D: Biol. Crystallogr.* **1994**, *D50*, 760–763; Vagin, A.; Teplyakov, A. MOLREP: an Automated Program for Molecular Replacement. *J. Appl. Crystallogr.* **1997**, *30*, 1022–1025.